OSU Oregon State UNIVERSITY

Open Access Articles

# *Conduction processes in metal–insulator–metal diodes with $Ta_2O_5$ and $Nb_2O_5$ insulators deposited by atomic layer deposition*

The Faculty of Oregon State University has made this article openly available.
Please share how this access benefits you. Your story matters.



| Citation | Alimardani, N., McGlone, J. M., Wager, J. F., & Conley Jr, J. F. (2013). Conduction processes in metal–insulator–metal diodes with $Ta_2O_5$ and $Nb_2O_5$ insulators deposited by atomic layer deposition. Journal of Vacuum Science & Technology A, 32(1), 01A122. doi:10.1116/1.4843555 |
| --- | --- |
| DOI | 10.1116/1.4843555 |
| Publisher | American Institute of Physics Publishing |
| Version | Version of Record |
| Terms of Use | http://cdss.library.oregonstate.edu/sa-termsofuse |



Oregon State UNIVERSITY OSU

# Conduction processes in metal–insulator–metal diodes with $Ta_2O_5$ and $Nb_2O_5$ insulators deposited by atomic layer deposition

Nasir Alimardani, John M. McGlone, John F. Wager, and John F. Conley, Jr.[a)]
*School of Electrical Engineering and Computer Science, Oregon State University, 1148 Kelley Engineering Center, Corvallis, Oregon 97331-5501*

(Received 19 September 2013; accepted 26 November 2013; published 13 December 2013)

Metal–insulator–metal diodes with $Nb_2O_5$ and $Ta_2O_5$ insulators deposited via atomic layer deposition are investigated. For both $Nb_2O_5$ and $Ta_2O_5$, the dominant conduction process is established as Schottky emission at small biases and Frenkel–Poole emission at large biases. Fowler–Nordheim tunneling is not found to play a role in determining current versus voltage asymmetry. The dynamic dielectric constants are extracted from conduction plots and found to be in agreement with measured optical dielectric constants. Trap energy levels at $\phi_T \approx 0.62$ and 0.53 eV below the conduction band minimum are estimated for $Nb_2O_5$ and $Ta_2O_5$, respectively. © *2014 American Vacuum Society*. [http://dx.doi.org/10.1116/1.4843555]

## I. INTRODUCTION

Recently, thin film metal–insulator–metal (MIM) tunnel devices have attracted significant attention for a variety of high-speed applications such as hot electron transistors,[1,2] infrared (IR) detectors,[3,4] and optical rectennas for IR energy harvesting.[5,6] Besides high-speed operation, additional MIM diode requirements for rectenna and IR detector applications include a small turn-on voltage ($V_{ON}$) for a low zero-bias resistance as well as asymmetric and nonlinear operation at low applied bias.[7] The ultrahigh frequency terahertz operation regime desired for these devices requires that the electron transport time between terminals be as short as a few femtoseconds. The standard way to achieve high speed rectification in an MIM diode is through Fowler–Nordheim tunneling (FNT) dominated charge transport in conjunction with the use of asymmetric work function metal electrodes which produce asymmetric, polarity dependent electron tunneling barriers.[8–10] Based on this principle of operation, insulators with a large electron affinity ($\chi$) appear to be desirable so as to produce small energy barriers at the metal electrodes and allow FNT to occur at small applied bias (low $V_{ON}$). Following this line of reasoning, it has been suggested that $Nb_2O_5$ and $Ta_2O_5$, insulators with large $\chi$, should be promising candidate insulators for rectenna applications.[11–13] In insulators with small barriers, FNT must compete with emission based conduction mechanisms such as Frenkel–Poole (FP) and Schottky emission. In fact, conduction in thick $Ta_2O_5$ films is often reported to be dominated by Frenkel–Poole, rather than FNT.

It is well known that deposition method can have a strong influence on electrical properties. Because MIM operation should be based on tunneling and tunneling is exponentially dependent on the barrier thickness, extremely uniform thickness control of the ultrathin insulating layer is required. Atomic layer deposition (ALD) is ideally suited for this application as it is based on self-saturating surface reactions which enable atomic scale control of thickness and uniformity over large surface areas and high aspect ratio structures. In addition, ALD allows deposition of high quality insulating films on a variety of metal electrodes, eliminating the need to use native oxides of rough polycrystalline metal electrodes. Recently, we demonstrated that combining high quality single layer and nanolaminate insulators deposited via ALD with ultrasmooth bottom electrodes enabled the realization of thin film MIM and metal–insulator–insulator–metal (MIIM) diodes with well-controlled quantum mechanical tunneling.[14–17] Although ALD processes for $Nb_2O_5$ or $Ta_2O_5$ have been reported, there are no reports on the electrical conduction of ALD $Nb_2O_5$ and no reports on $Ta_2O_5$ in MIM structures with atomically smooth amorphous metal bottom electrodes, and it is not known whether these insulators will support FNT-based operation.

In this work, we investigate ALD $Nb_2O_5$ and $Ta_2O_5$ insulating tunnel barriers (I) in $M_1IM_2$ diodes fabricated with atomically smooth ZrCuAlNi amorphous bottom electrodes ($M_1$) and Al top electrodes ($M_2$). The current density versus voltage (J–V) characteristics and rectification behavior are studied at temperatures ranging from 300 to 375 K and the dominant conduction mechanisms are identified in different bias regimes.

## II. EXPERIMENT

MIM diodes were fabricated on Si substrates capped with 100 nm of thermally grown $SiO_2$. A 150 nm thick amorphous metal ZrCuAlNi (ZCAN) bottom electrode was deposited directly on the $SiO_2$ via DC magnetron sputtering using a $Zr_{40}Cu_{35}Al_{15}Ni_{10}$ metal target. The RMS and peak roughness of the ZCAN blanket film were measured to be 0.3 and 3 nm, respectively.[14] Next, thin 5 and 10 nm thick insulators were deposited via ALD using a Picosun SUNALE R-150B. Tantalum ethoxide [$Ta_2(OC_2H_5)_{10}$] and niobium ethoxide [$Nb_2(OC_2H_5)_{10}$] were used as the metal organic precursors for $Ta_2O_5$ and $Nb_2O_5$, respectively. Both ALD films were deposited at a chamber temperature of 250 °C using deionized water as the oxidant. Finally, Al top electrode dots (~0.2 mm$^2$) were formed via evaporation using a shadow mask.

The thickness of the insulating films on Si was measured with a J. A. Woollam WVASE32 spectroscopic ellipsometer

[a)]Electronic mail: jconley@eecs.oregonstate.edu



Redistribution subject to AVS license or copyright; see http://scitation.aip.org/termsconditions. Download to IP: 128.193.163.187 On: Fri, 06 Jun 2014 21:18:47

using a Cauchy model. High frequency optical dielectric constants were determined with spectroscopic ellipsometry using 10 nm thick films deposited on silicon substrates. The crystal structure was assessed with x-ray diffraction (XRD) using a Bruker-AXS D8 Discover x-ray diffractometer. Both the $Ta_2O_5$ and $Nb_2O_5$ ALD thin films were found to be almost entirely amorphous as-deposited; however, the presence of nanocrystalline seeds could be expected. Crystalline phases in thin insulating films may create alternate conduction paths for electrons.[18] Crystallization of the bottom electrode increases roughness which can result in electric field enhancement,[19] increased defect density at the insulator–electrode interface,[20] and work function nonuniformity due to different orientations of crystalline grains.[21] To avoid any possibility of crystallization of either the ALD films or the ZrCuAlNi bottom electrode, all devices were studied without postdeposition annealing.

Electrical measurements were conducted on a thermal chuck at temperatures ranging from 300° K to 375° K using a TEMPTRONIC gold plated ThermoChuck and a probe station in a dark box using an Agilent 4156C semiconductor parameter analyzer; the noise floor of this system is estimated to be on the order of $10^2$ pA. The ZrCuAlNi bottom electrode was always held at ground with bias applied to the Al top gate. To mitigate the impact of displacement current, all I–V curves were swept from zero-bias to either the maximum positive or negative bias. Two figures of merit were used to characterize the devices: (i) I–V asymmetry, $\eta_{asym}$, is defined as negative device current divided by positive current $|I_-/I_+|$ so that $\eta_{asym} = 1$ indicates symmetric operation and (ii) nonlinearity, $f_{NL}$, is defined as (dI/dV)/(I/V). Many individual devices of each of the four types of device structures were measured. Representative results are discussed.

Band diagrams were simulated using the Boise State University Band Diagram program.[22] Materials parameters used in simulation are electron affinity ($\chi$) = 4 eV, bandgap ($E_G$) = 4.3 eV, and relative dielectric constant ($\kappa$) = 28 for $Nb_2O_5$;[23,24] $\chi = 3.75$ eV, $E_G = 4.4$ eV, and $\kappa = 24$ for $Ta_2O_5$.[24,25] The work function of the ZrCuAlNi and Al electrodes were determined to be 4.8 and 4.2 eV, respectively, as reported in our previous work.[17]

## III. RESULTS AND DISCUSSION

Shown in Fig. 1 are log (J)–V plots of $M_1IM_2$ diodes made with (a) 10 nm thick and (b) 5 nm thick layers of either as-deposited $Ta_2O_5$ or as-deposited $Nb_2O_5$. Plots of $\eta_{asym}$ versus voltage and $f_{NL}$ versus voltage for all devices are shown in Figs. 1(c) and 1(d), respectively. The leakage current density of the 10 nm $Ta_2O_5$ films is comparable to that previously reported for ALD $Ta_2O_5$ in MIS structures.[26,27] As expected, based on the relative barrier heights shown in the simulated energy band-diagrams inset of Fig. 1(a), devices made using $Nb_2O_5$ show a larger current density than devices made using $Ta_2O_5$. The $Ta_2O_5$ diodes, however, show slightly larger asymmetry. Although $Ta_2O_5$ and $Nb_2O_5$ devices both show asymmetric J–V behavior with a small $V_{ON}$, the maximum asymmetry ($\eta_{max}$) is three orders of

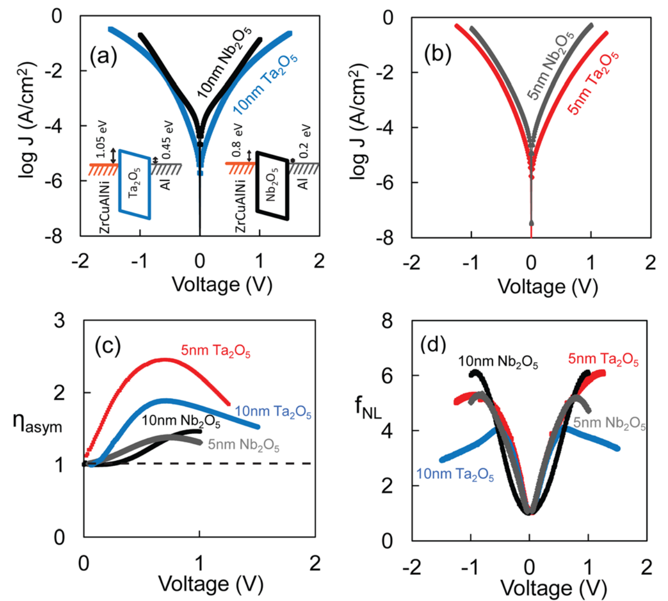


FIG. 1. (Color online) Log (J) vs V plots for $M_1IM_2$ diodes made with ZrCuAlNi bottom electrodes and Al top electrodes with (a) 10 nm of $Nb_2O_5$ and $Ta_2O_5$ insulators, and (b) 5 nm of $Nb_2O_5$ and $Ta_2O_5$ insulators. (c) Asymmetry ($\eta_{asym}$) plots and (d) nonlinearity ($f_{NL}$) plots of diodes shown in (a) and (b). Insets in (a) illustrates energy band diagrams of $Nb_2O_5$ and $Ta_2O_5$ $M_1IM_2$ in equilibrium.

magnitude smaller than the $\eta_{max}$ (up to 1400), which we have recently reported for diodes with a 10 nm $Al_2O_3$ insulator layer made using the same electrode combination.[17] The asymmetry in an $M_1IM_2$ tunnel diode should be related to the work function difference between the electrodes ($\Delta\Phi = \Phi_{M1} - \Phi_{M2}$). Theoretically, if conduction is assumed to be dominated solely by FNT, devices made with the same electrodes but different insulators should show the same value of $\eta_{max}$, but at different applied biases depending on the electron affinity of the insulator (e.g., energy barrier heights formed at the electrode interfaces). The poor asymmetric behavior shown in Fig. 1(c) suggests that charge transport through these films may include processes other than FNT, although there are many nonideal factors that could also impact asymmetry including interface states, roughness, defects, and presence of other conduction. Fowler–Nordheim plots of $\ln(J/V^2)$ vs 1/V show poor linearity ($R^2 < 0.95$), confirming that FNT does not dominate conduction in either insulator.

Besides FNT and direct tunneling (which should be suppressed in the thicker 10 nm thick films), possible competing conduction mechanisms include Schottky emission (SE), Frenkel–Poole emission (FPE), and space-charge-limited (SCL) conduction. SCL is ruled out because J does not exhibit a $V^2$ dependence.[28] In SE, conduction is limited by emission over a barrier and the current density, $J_{SE}$, has the following relationship with electric field, E:[10]

$$J_{SE} = A^*T^2 \exp\left[\frac{-q(\Phi_B - \sqrt{qE/4\pi\kappa_r\varepsilon_0}}{\kappa T}\right], \tag{1}$$

where A* is the effective Richardson constant, T is temperature, q is the elementary charge, $\Phi_B$ is the barrier height



Redistribution subject to AVS license or copyright; see http://scitation.aip.org/termsconditions. Download to IP: 128.193.163.187 On: Fri, 06 Jun 2014 21:18:47

between the Fermi-level of the injecting metal and the conduction band minimum of the insulator, $\kappa_r$ is the optical dielectric constant, $\varepsilon_0$ is the permittivity in vacuum, and k is Boltzmann's constant. For FPE, where conduction is limited by emission from traps, the relationship between $J_{FPE}$ and E is[10]

$$J_{FPE} = E \exp\left[\frac{-q\left(\phi_T - \sqrt{qE/\pi\kappa_r\varepsilon_0}\right)}{kT}\right], \tag{2}$$

where $\phi_T$ is the trap energy depth referenced to the insulator conduction band minimum.

As a first step toward determining whether the dominant conduction mechanism is related to SE or FPE, the J–V data from Fig. 1(a) were replotted as ln $(I_{SE}/T^2)$ vs $V^{1/2}$ and ln $(I_{FPE}/V)$ vs $V^{1/2}$, respectively. Shown in Fig. 2, it was found that the 10 nm thick $Ta_2O_5$ and $Nb_2O_5$ devices in Fig. 2(a) as well as the 5 nm thick $Ta_2O_5$ and $Nb_2O_5$ devices in Fig. 2(b) produced linear ln $(I/T^2)$ vs $V^{1/2}$ curves ($R^2 > 0.999$) at both polarities at low biases (0.1 to 0.3 V), suggesting that SE dominates in the low bias regime. At higher biases (0.75 to 1 V), both the 10 nm thick $Ta_2O_5$ and $Nb_2O_5$ devices in Fig. 2(c), and the 5 nm thick $Ta_2O_5$ and $Nb_2O_5$ devices in Fig. 2(d) produced linear ln (I/V) vs $V^{1/2}$ plots, suggesting that FPE dominates at higher biases. The change in the dominant conduction mechanism from SE limited at low biases to FPE limited at high biases is consistent with the observed asymmetry in these devices. As shown in Fig. 1(c), asymmetry first increases in the low bias regime where the electrode-limited (asymmetric) SE dominates and then decreases at larger biases where bulk-limited (symmetric) FPE dominates.

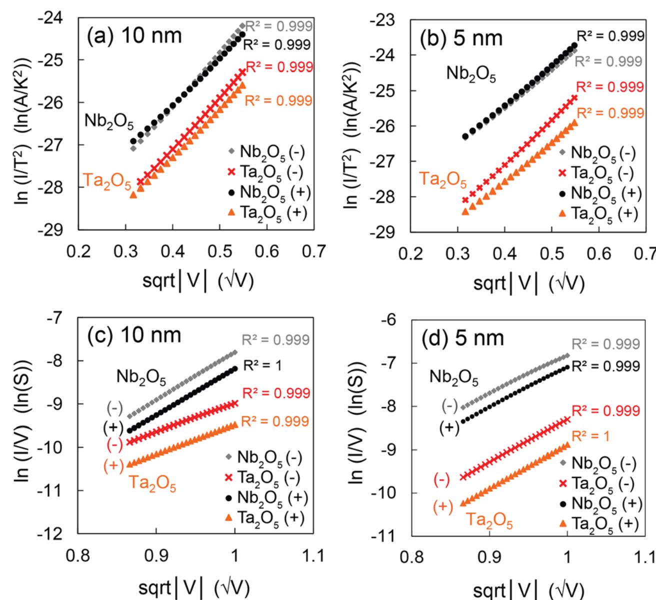


FIG. 2. (Color online) Schottky plots in (a) and (b) for the low voltage regime ($V_{appl} = 0.1$ V to approximately 0.3 V) and Frenkel–Poole plots in (c) and (d) for the higher voltage regime ($V_{appl} = 0.75$ V to approximately 1 V) show highly linear curves with $R^2 > 0.999$ for both 5 nm [shown in (b) and (d)] and 10 nm [shown in (a) and (c)] $Nb_2O_5$ and $Ta_2O_5$ diodes.

As the linearity of conductions plots is insufficient to unambiguously assign conduction mechanisms, to further assess the validity of these provisional conduction mechanism assignments, the dynamic relative dielectric constants, $\kappa_r$, of $Nb_2O_5$ and $Ta_2O_5$ were extracted from the slopes of the plots in Fig. 2. For $Nb_2O_5$, $\kappa_r = 4.7 \pm 0.3$ was extracted from the SE plot in Figs. 2(a) and 2(b), and $\kappa_r = 5.5 \pm 0.1$ from FPE plot in Figs. 2(c) and 2(d). For $Ta_2O_5$, $\kappa_r = 4.0 \pm 0.3$ was extracted from the SE plot in Figs. 2(a) and 2(b) and $\kappa_r = 4.6 \pm 0.1$ from the FPE plot in Figs. 2(c) and 2(d). For both $Nb_2O_5$ and $Ta_2O_5$, the values of $\kappa_r$ are essentially the same for both polarities and for both 5 and 10 nm thick films. As expected, these extracted dynamic dielectric constants are much smaller than the static dielectric constants measured for each film. Using the capacitance versus voltage technique, we previously[29] reported $\kappa = 24$ for $Ta_2O_5$ consistent with reports for amorphous ALD $Ta_2O_5$.[25] For $Nb_2O_5$, $\kappa = 24$–$26$ is measured in reasonable agreement with values reported for amorphous $Nb_2O_5$ in which $Nb(NEt_2)_3$ was used as the ALD precursor.[23] Although the static or DC dielectric constant is sometimes used erroneously in the assignment of FPE, it is the dynamic or optical dielectric constant that should be used.[30–33] The dielectric constant associated with FPE current under relatively large electric field is expected to have the high frequency value as emission of electrons from the traps should occur at times corresponding to optical frequencies.[30,31] In his original work, Frenkel used the optical dielectric constant to derive what is now called the Frenkel–Poole emission equation [Eq. (2)].[34] Using spectroscopic ellipsometry, we measure the optical dielectric constant ($n^2$) in the wavelength range of 400–1200 nm to range from 5.5 to 6.2 for $Nb_2O_5$ and from 4.6 to 4.95 for $Ta_2O_5$. The index of refraction, n, measured via ellipsometry at wavelength of 580 nm for $Ta_2O_5$ is 2.28, consistent with $n = 2.2$–$2.3$ reported for ALD deposited $Ta_2O_5$.[35] For ALD $Nb_2O_5$, $n = 2.39$ at 580 nm measured. The $\kappa_r$ values extracted from the FPE plots ($5.5 \pm 0.1$ for $Nb_2O_5$ and $4.6 \pm 0.1$ for $Ta_2O_5$), both match well with the range of values measured optically, supporting the assignment of FPE as the dominant mechanism at higher biases. For the SE plots, the extracted $\kappa_r$ values ($4.7 \pm 0.3$ for $Nb_2O_5$ and $4.0 \pm 0.3$ for $Ta_2O_5$) are somewhat below the range of the optical dielectric constants, but still match reasonably well, so that the designation of SE is more tentative.

Figure 3 shows (a) log J–V, (b) $\eta_{asym}$, and (c) $f_{NL}$ plots for 10 nm $Nb_2O_5$ diodes, along with (d) log J–V, (e) $\eta_{asym}$, and (f) $f_{NL}$ plots for 10 nm $Ta_2O_5$ diodes at temperatures ranging from 300 to 375 K. The strong temperature dependence exhibited by the J–V characteristics of both the $Nb_2O_5$ and $Ta_2O_5$ [Figs. 3(a) and 3(d), respectively] devices provides additional evidence for the dominance of a thermal emission mechanism and further rules out FNT, which should not exhibit strong temperature dependence, as a dominant conduction mechanism. Shown in Fig. 3, $\eta_{max}$, as well as the voltage at which $\eta_{max}$ occurs, decreases as temperature increases for both the (b) $Nb_2O_5$ and (e) $Ta_2O_5$ devices. A similar trend is observed for the $f_{NL}$ plots for both devices. Similar results are also seen for the 5 nm thick diodes. This



Redistribution subject to AVS license or copyright; see http://scitation.aip.org/termsconditions. Download to IP: 128.193.163.187 On: Fri, 06 Jun 2014 21:18:47

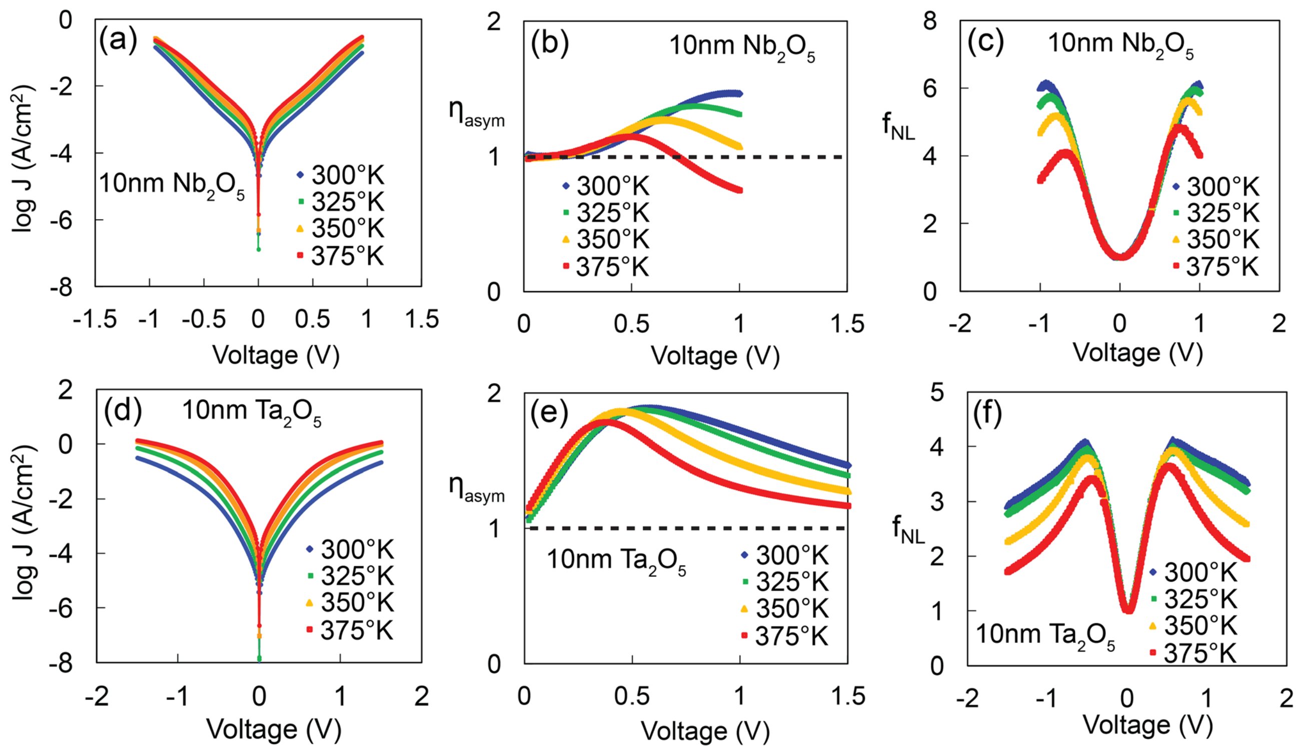


FIG. 3. (Color online) (a) Log (J) vs V plots, (b) asymmetry ($\eta_{asym}$) plots, and (c) nonlinearity ($f_{NL}$) plots of 10 nm $Nb_2O_5$ diodes at different temperatures. (d) Log J vs V plots, (e) asymmetry ($\eta_{asym}$) plots, and (f) nonlinearity ($f_{NL}$) plots of 10 nm $Ta_2O_5$ diodes at different temperatures.

may be explained as follows. Conduction limited by SE [Eq. (1)] has a stronger temperature dependence than FPE [Eq. (2)]. Therefore, SE should become relatively stronger as compared to FPE as the temperature increases. Assuming that SE and FPE are modeled as operating in series, conduction should become increasingly limited (dominated) by FPE as temperature increases. Whereas SE is dependent on the height of the barrier at the metal/insulator interface and thus would be expected to be asymmetric with respect to voltage polarity for these asymmetric electrode devices, FPE is a bulk conduction mechanism and should be symmetric with respect to voltage polarity. The observed behavior of decreasing asymmetry with increasing temperature is thus consistent with an increased dominance of FPE with increasing temperature.

FPE is characterized by the energy depth of the dominant trap, $\phi_T$, which is referenced to the conduction band minimum or valance band maximum for n-type and p-type materials, respectively. Shown in Fig. 4 are plots of the extracted $E_a$ versus the square root of the voltage across the insulator for the voltage region (0.7 to 1 V) in which FPE appears to be dominant in both $Nb_2O_5$ and $Ta_2O_5$. The value of $E_a$ at each voltage was extracted from Arrhenius plots of ln (I/V) vs 1/kT for the 5 and 10 nm thick $Nb_2O_5$ and $Ta_2O_5$ diodes. To account for the Schottky barrier lowering of the trap depth when a field is applied across the insulator, the zero field trap depth, $\phi_T$, is estimated by extrapolating the plots in Fig. 4 to V = 0. The extracted $\phi_T$ values are considered to be below the conduction band minimum as both $Nb_2O_5$ and $Ta_2O_5$ have been reported to be n-type materials.[36–38] Considering first $Ta_2O_5$, $\phi_T$ was estimated to be 0.53 ± 0.05 eV below the conduction band minimum. This value is in reasonable agreement with the $\phi_T = 0.7$ eV reported by Houssa *et al.* for ALD $Ta_2O_5$ deposited using $TaCl_5$ as the precursor.[39] The 0.17 eV difference could be due to the different ALD precursors used in the present study. For example, Houssa *et al.* elsewhere reported $\phi_{T0} = 0.85$ eV for $Ta_2O_5$ films deposited using metal organic

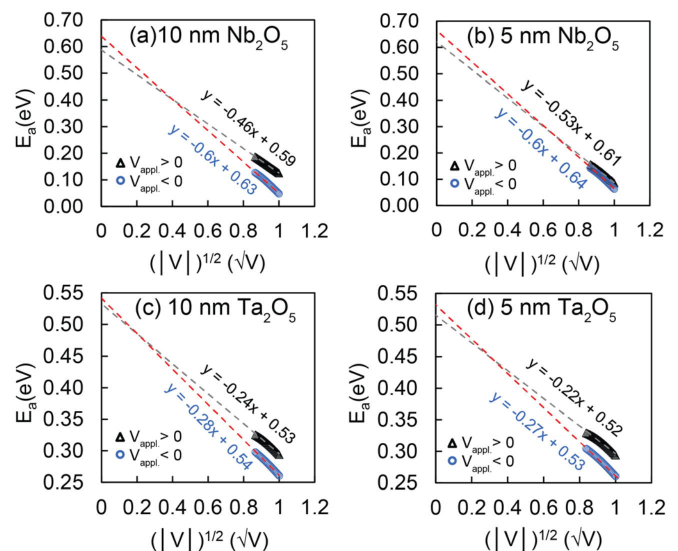


FIG. 4. (Color online) Plots of $E_a$ vs sqrt |V| in the Frenkel–Poole dominated bias regime ($V_{appl} = 0.7$ to 1 V) for (a) 10 nm $Nb_2O_5$ diodes, (b) 5 nm $Nb_2O_5$ diodes, (c) 10 nm $Ta_2O_5$ diodes, and (d) 5 nm $Ta_2O_5$ diodes. The trap depth, $\phi_{T0}$, is extracted by extrapolation of the curves to zero bias. All the curves used for extrapolating trap depths are linear with $R^2 > 0.99$.



Redistribution subject to AVS license or copyright; see http://scitation.aip.org/termsconditions. Download to IP: 128.193.163.187 On: Fri, 06 Jun 2014 21:18:47

chemical vapor deposition (MOCVD).[40] Recent *ab-initio* calculations predict an $\phi_T$ of 0.2 eV for $\delta$-$Ta_2O_5$.[41] For $Nb_2O_5$, the $\phi_T$ was found to be $0.62 \pm 0.05$ eV below the conduction band minimum. Reports on conduction mechanisms in thin film ALD $Nb_2O_5$ using $Nb_2(OC_2H_5)_{10}$ are limited. For comparison García *et al*. have recently reported $\phi_T = 0.8$ eV for annealed $Nb_2O_5$ films deposited by PEALD with $Nb(Net_2)_3$ precursor.[23] Note that for both $Nb_2O_5$ and $Ta_2O_5$, the extracted trap depths were the same for both positive and negative bias and were similar for both 5 and 10 nm films, further evidence that FPE is indeed dominant in this bias region.

## IV. SUMMARY AND CONCLUSIONS

In summary, asymmetric metal electrode $M_1IM_2$ diodes comprising atomically smooth amorphous ZrCuAlNi bottom electrodes, high electron affinity $Nb_2O_5$ and $Ta_2O_5$ insulators as-deposited via ALD, and Al top electrodes were investigated. The I–V characteristics and device performance were measured at temperatures ranging from 300 to 375 K and the dominant conduction mechanisms were identified in different bias regimes. For both insulators, it was found that SE dominates at low biases whereas FPE dominates at larger biases. Using FPE analysis, the dominant "bulk" trap depths were estimated to be $0.53 \pm 0.05$ eV below the conduction band minimum for $Ta_2O_5$ and $0.62 \pm 0.05$ eV for $Nb_2O_5$. $Nb_2O_5$ and $Ta_2O_5$ have been considered to be promising insulators for high speed MIM devices. However, conduction in both insulators deposited via ALD was found to be dominated by thermal emission, rather than tunneling based mechanisms. Although in principle thermal emission at high electric fields can be fast (possibly of order 10 s of THz as assessed from spectroscopic ellipsometry), FPE-dominated conduction does not provide asymmetry as the traps behave in the same manner under positive and negative bias. If asymmetric work function electrodes are used to produce different barrier heights, interface-dominated SE can provide low voltage asymmetry. However, the exponential temperature dependence of SE makes it unsuitable for applications where careful temperature control is not viable. FNT, in contrast, offers inherently fast transport times and does not suffer from a strong temperature dependence, making it a more desirable mechanism for high-speed device operation. Recently, we demonstrated that by using nanolaminate bilayer tunnel barrier MIIM devices, step-tunneling may be used to tune asymmetry and nonlinearity.[17] It has been predicted, based on theoretically considerations, that $Nb_2O_5/Ta_2O_5$ bilayers should be promising insulator candidates for MIIM devices for rectenna applications.[12,13] Although it may be possible to reduce the magnitude of leakage current in these insulators through post deposition annealing, plasma processing, or alternate choice of precursors, the fact that tunnel based conduction does not play a dominant role in either as deposited ALD $Nb_2O_5$ or $Ta_2O_5$ suggests that this insulator combination will not be able to support the step tunneling mechanism that was exploited to improve asymmetry and reduce $V_{ON}$ in MIIM diodes in our previous work.[17] In conclusion, although their large electron affinities make $Nb_2O_5$ and $Ta_2O_5$ seem attractive for MIM applications, because Fowler–Nordheim tunneling does not appear to play a significant role in device operation, ultra-high frequency applications of ALD $Nb_2O_5$- or ALD $Ta_2O_5$-based MIM devices may be limited.

## ACKNOWLEDGMENTS

This work was supported in part by grants from the National Science Foundation through DMR-0805372 and CHE-1102637, the U.S. Army Research Laboratory through W911NF-07-2-0083, and matching support from the Oregon Nanoscience and Microtechnologies Institute (ONAMI). The authors thank Ram Ravichandran for performing spectroscopic ellipsometry and C. Tasker for equipment support.

[1]S. Vaziri, G. Lupina, C. Henkel, A. D. Smith, M. Östling, J. Dabrowski, G. Lippert, W. Mehr, and M. C. Lemme, Nano Lett. **13**, 1435 (2013).
[2]C. Zeng, E. B. Song, M. Wang, S. Lee, C. M. Torres, Jr., J. Tang, B. H. Weiller, and K. L. Wang, Nano Lett. **13**, 2370 (2013).
[3]P. Maraghechi, A. Foroughi-Abari, K. Cadien, and A. Y. Elezzabi, Appl. Phys. Lett. **100**, 113503 (2012).
[4]P. C. D. Hobbs, R. B. Laibowitz, F. R. Libsch, N. C. LaBianca, and P. P. Chiniwalla, Opt. Express **15**, 16376 (2007).
[5]R. Corkish, M. A. Green, and T. Puzzer, Sol. Energy, **73**, 395 (2002).
[6]S. Joshi and G. Moddel, Appl. Phys. Lett. **102**, 083901 (2013).
[7]N. M. Miskovsky, P. H. Cutler, A. Mayer, B. L. Weiss, B. Willis, T. E. Sullivan, and P. B. Lerner, J. Nanotechnol. **2012**, 512379 (2012).
[8]J. G. Simmons, J. Appl. Phys. **34**, 2581 (1963).
[9]H. Ekurt and A. Hahn, J. Appl. Phys. **51**, 1686 (1980).
[10]S. M. Sze and K. K. Ng, *Physics of Semiconductor Devices*, 3rd ed. (Wiley-Interscience, Hoboken, NJ, 2007).
[11]P. Periasamy, J. J. Berry, A. A. Dameron, J. D. Bergeson, D. S. Ginley, R. P. O'Hayre, and P. A. Parilla, Adv. Mater. **23**, 3080 (2011).
[12]S. Grover and G. Moddel, IEEE J. Photovolt. **1**, 78, (2011).
[13]E. I. Hashem, N. H. Rafat, and E. A. Soliman, IEEE J. Quantum Electron. **49**, 72 (2013).
[14]N. Alimardani, E. W. Cowell III, J. F. Wager, J. F. Conley, Jr., D. R. Evans, M. Chin, S. J. Kilpatrick, and M. Dubey, J. Vac. Sci. Technol. A **30**, 01A113 (2012).
[15]E. W. Cowell III, N. Alimardani, C. C. Knutson, J. F. Conley, Jr., D. A. Keszler, B. J. Gibbons, and J. F. Wager, Adv. Mater. **23**, 74 (2011).
[16]N. Alimardani, J. F. Conley, Jr., E. W. Cowell III, J. F. Wager, M. Chin, S. Kilpatrick, and M. Dubey, in *IEEE International Integrated Reliability Workshop (IRW) Final Report* (IEEE, 2010), p. 80.
[17]N. Alimardani and J. F. Conley, Jr., Appl. Phys. Lett. **102**, 143501 (2013).
[18]T. Usui, S. A. Mollinger, A. T. Iancu, R. M. Reis, and F. B. Prinz, Appl. Phys. Lett. **101**, 033905 (2012).
[19]K. Choi, F. Yesilkoy, G. Ryu, S. H. Cho, N. Goldsman, M. Dagenais, and M. Peckerar, IEEE Trans. Electron Devices **58**, 3519 (2011).
[20]S. K. Kim, S. W. Lee, J. H. Han, B. Lee, S. Han, and C. S. Hwang, Adv. Funct. Mater. **20**, 2989 (2010).
[21]M. E. Grubbs, X. Zhang, M. Deal, Y. Nishi, and B. M. Clemens, Appl. Phys. Lett. **97**, 223505 (2010).
[22]R. G. Southwick III, A. Sup, A. Jain, and W. B. Knowlton, IEEE Trans. Device Mater. Reliab. **11**, 236 (2011).
[23]H. García, H. Castán, E. Perez, S. Dueñas, L. Bailón, T. Blanquart, J. Niinistö, M. Ritala, and M. Leskelä, Semicond. Sci. Technol. **28**, 055005 (2013).
[24]J. Robertson, J. Vac. Sci. Technol. B **18**, 1785 (2000).
[25]K. Kukli, J. Ihanus, M. Ritala, and M. Leskelä, J. Electrochem. Soc. **144**, 300 (1997).
[26]T. Aoyama, S. Saida, Y. Okayama, M. Fujisaki, K. Imai, and T. Arikado, J. Electrochem. Soc. **143**, 977 (1996).
[27]D. Gu, J. Li, S. K. Dey, H. De Waard, and S. Marcus, J. Vac. Sci. Technol. B **24**, 2230 (2006).
[28]A. Rose, Phys. Rev. **97**, 1538 (1955).
[29]S. W. Smith, K. McAuliffe, and J. F. Conley, Jr., Solid-State Electron. **54**, 1076 (2010).



Redistribution subject to AVS license or copyright; see http://scitation.aip.org/termsconditions. Download to IP: 128.193.163.187 On: Fri, 06 Jun 2014 21:18:47

[30]D. S. Jeong and C. S. Hwang, J. Appl. Phys. **98**, 113701 (2005).
[31]R. Ludeke, M. T. Cuberes, and E. Cartier, Appl. Phys. Lett. **76**, 2886 (2000)
[32]M. Specht, M. Stadele, S. Jakschik, and U. Schroder, Appl. Phys. Lett. **84**, 3076 (2004).
[33]O. Blank, H. Reisinger, R. Stengl, M. Gutsche, F. Wiest, V. Capodieci, J. Schulze, and I. Eisele, J. Appl. Phys. **97**, 044107 (2005).
[34]J. Frenkel, Phys. Rev. **54**, 647 (1938).
[35]K. Kukli, M. Ritala, R. Matero, and M. Leskelä, J. Cryst. Growth **212**, 459 (2000).
[36]Ç. Kiliç and A. Zunger, Appl. Phys. Lett. **81**, 73 (2002).
[37]I. Nowak and M. Ziolek, Chem. Rev. **99**, 3603 (1999).
[38]W. S. Lau, T. S. Tan, N. P. Sandler, and B. S. Page, Jpn. J. Appl. Phys., Part 1 **34**, 757 (1995).
[39]M. Houssa, M. Tuominen, M. Naili, V. Afanas'ev, A. Stesmans, S. Haukka, and M. M. Heyns, J. Appl. Phys. **87**, 8615 (2000).
[40]M. Houssa, R. Degraeve, P. W. Mertens, M. M. Heyns, J. S. Jeon, A. Halliyal, and B. Ogle, J. Appl. Phys. **86**, 6462 (1999).
[41]M. V. Ivanov, T. V. Perevalov, V. S. Aliev, V. A. Gritsenko, and V. V. Kaichev, J. Appl. Phys. **110**, 024115 (2011).



Redistribution subject to AVS license or copyright; see http://scitation.aip.org/termsconditions. Download to IP: 128.193.163.187 On: Fri, 06 Jun 2014 21:18:47